Demonstration of Half-Metallicity in Fermi-Level-Tuned Heusler Alloy $Co_2FeAl_{0.5}Si_{0.5}$ at Room Temperature

R. Shan, H. Sukegawa, W. H. Wang, M. Kodzuka, T. Furubayashi, T. Ohkubo, S. Mitani, K. Inomata, and K. Hono

Magnetic Materials Center, National Institute for Materials Science (NIMS), 1-2-1 Sengen, Tsukuba, 305-0047, Japan

(Received 11 March 2009; published 15 June 2009)

Fermi level tuning has been successfully demonstrated in Co-based full-Heusler alloy $Co_2FeAl_{0.5}Si_{0.5}$ (CFAS). The half-metallic band gap of CFAS was proved by the behavior of differential conductance of CFAS/$(MgAl_2)O_x$/CoFe magnetic tunneling junctions with an unexplored crystalline $(MgAl_2)O_x$ barrier. CFAS exhibits the highest effective spin polarization ($P_{\rm eff}$) at 300 K and the weakest temperature dependence of $P_{\rm eff}$ among all known half metals. Further study shows that $P_{\rm eff}$ of CFAS decays with increasing temperature (T) following $T^{3/2}$ law perfectly, which indicates that the depolarization of CFAS is determined by spin wave excitation only.

DOI: 10.1103/PhysRevLett.102.246601 PACS numbers: 72.25.−b, 75.47.−m, 75.50.−y

Half-metals can be considered as the ideal materials for spintronics, since the efficiency of spin-dependent devices will be largest if the current is 100% spin polarized [1]. However, the strong temperature dependence of spin polarization (P) of all reported half-metallic materials, mainly due to spin wave excitation [2–4] and the narrow energy separation between the Fermi level and the conduction or valence band edge [5,6], limits their practical applications. As a promising candidate of half-metal, Co-based full-Heusler alloys attract broad interest in the last decade because of their high magnetization and high Curie temperature [7–18]. Recently, Sakuraba *et al.* [7,17,18] reported a series of exciting results about Co_2MnSi (CMS) and proved its half-metallic character at a low temperature. Unfortunately, the spin polarization of CMS still has a strong temperature dependence possibly resulting from the narrow energy separation between the Fermi level and the bottom edge of the conduction band of CMS. Almost at the same time, some groups [14–16] were aware that the Fermi level position of ternary Heusler alloy could be tuned by doping a fourth element. However, experimental evidence has been absent until now because of the perplexing relationship between P and the structure disorder of quaternary Co-based full-Heusler alloy. Here, we report a new half-metallic material applying Fermi level tuning experimentally, the quaternary Co-based full-Heusler alloy $Co_2FeAl_{0.5}Si_{0.5}$ (CFAS), which exhibits a high P above 0.9, although those for Co_2FeAl and Co_2FeSi were reported only around 0.5 and 0.6 at a low temperature, respectively [8]. CFAS exhibits the weakest temperature dependence of spin polarization among all known half-metals, which is attributed to the Fermi level position of CFAS locating in the middle of the large band gap. Similar to the doping techniques in semiconductors, Fermi level tuning means that the electronic structure of certain materials could be adjusted by doping to obtain the desired property, and thus may lead to the development of new families of half-metal with better performance.

In this study, tunneling magnetoresistance (TMR) effect is adopted to evaluate spin polarization, since it can be deduced using Julliere's model [19] at various temperatures. The TMR ratio is defined as $(R_{Ap} - R_P)/R_P$, where R_{Ap} and R_P are the tunnel resistance when the magnetizations of the two electrodes are aligned in antiparallel and parallel, respectively. Thin films for spin valve type CFAS/$(MgAl_2)O_x$/CoFe magnetic tunneling junctions (MTJs) and CoFe/$(MgAl_2)O_x$/CoFe MTJs were prepared using magnetron sputtering with a base pressure of 4×10^{-7} Pa except for Al layer. All layers were deposited at room temperature. The CFAS full-Heusler alloy film was grown from a stoichiometric Co-Fe-Al-Si (Co: 50%, Fe: 25%, Al: 12.5%, Si: 12.5%) target. For CFAS/$(MgAl_2)O_x$/CoFe MTJs, a stacking structure of Cr(40)/$Co_2FeAl_{0.5}Si_{0.5}$(80) / $(MgAl_2)O_x$[0.7(Mg) + 1.3(Al)] / $Co_{75}Fe_{25}$(3)/$Ir_{22}Mn_{78}$(12)/Ru(7), where the numbers are the layer thicknesses in nanometers, was employed. Thermal treatment *in situ*: MgO(001) substrate was heated at 800 °C; Cr buffer layer was annealed at 800 °C; CFAS layer was annealed at 430 °C to obtain a perfect $B2$ structure. Al layer was deposited at the oxidization chamber with a base pressure of 2×10^{-6} Pa. The $(MgAl_2)O_x$ tunnel barrier was formed by inductively coupled plasma treatment for 120 s in a mixture of Ar + O_2 atmosphere (7.0 Pa). The whole sample was annealed at 290 °C for 10 min *ex situ* and cooled down to room temperature naturally in vacuum (1×10^{-4} Pa) under a magnetic field of 3000 Oe. For CoFe/$(MgAl_2)O_x$/CoFe MTJs, thin films were prepared on Si/SiO_2 substrate. The stacking structure of samples is as follows: Ru(7)/IrMn(12)/CoFe(3)/$(MgAl_2)O_x$(0.7 + 1.3)/CoFe(3)/Ru(7), with thicknesses in nanometers. The growth and oxidization conditions of $(MgAl_2)O_x$ tunneling barrier for CoFe/$(MgAl_2)O_x$/CoFe MTJs are the same as those for CFAS/$(MgAl_2)O_x$/CoFe MTJs. The post-annealing temperature in a magnetic field for CoFe/$(MgAl_2)O_x$/CoFe MTJs is 250 °C. Junctions with an area of $10 \times 10\ \mu m^2$ were made by microfabrication techniques in a clean room.

 © 2009 The American Physical Society

Typical resistance versus field curves of CFAS/$(MgAl_2)O_x$/CoFe MTJs measured at 7, 26, and 300 K by the four-probe magnetoresistance (MR) measurement system are shown in Fig. 1(a). A bias voltage of 1.2 mV was applied for measurement at 300 K, while 2.5 mV for measurements at 26 and 7 K. A TMR ratio of 102.3% at room temperature was achieved, which is the highest in MTJs with non-MgO barrier. The TMR ratio reaches the maximum (162%) at 26 K and then decreases slightly with lowering measurement temperature. The reduction of TMR ratio is probably ascribed to the incomplete antiparallel magnetization state between the free layer and pinned layer resulting from the coercivity enhancement of the free CFAS layer at a very low temperature.

Figure 1(b) shows the dependence of differential conductance on bias voltage (dI/dV-V) of CFAS/$(MgAl_2)O_x$/CoFe MTJs at 7 and 300 K. Here, a negative bias voltage means that electrons are tunneling from CFAS to CoFe. Obvious asymmetry of $G = dI/dV$ curves for the parallel configuration [$G_P(V)$] with respect to the polarity of bias voltage was observed at both 7 and 300 K. The critical voltages (V_c) corresponding to the minimum $G_P(V)$ at 7 and 300 K are -320 and -290 mV, respectively. As shown by the illustration A and B in Fig. 1(c), when the bias voltage $V < -|V_c|$, both channels of the majority spins and the minority spins in the MTJs will open, and thus $G_P(V)$ increases rapidly [17]. In view of the contribution of thermal fluctuation, the difference of $|V_c|$ between 0 and 300 K should be equal to $|k_BT/e| \approx$ 26 mV, where k_B is the Boltzmann constant and e is the charge of electron. Here, our data (~30 meV) is highly consistent with the theoretical analysis and reveals the large energy separation between the Fermi level and the top of the valence band in CFAS. Besides, the rapid increasing of $G_P(V)$ in positive bias voltage range was suggested to reflect a narrow energy separation between the Fermi level and the bottom of the conduction band [17]. However, we found that $G_P(V)$ of CFAS/$(MgAl_2)O_x$/CoFe MTJs are almost parallel with that of CoFe/$(MgAl_2)O_x$/CoFe MTJs in a large range of positive bias voltage, as shown in the inset of Fig. 1(b), which possibly implies that $G_P(V)$ in this bias voltage range mainly reflect the property of CoFe rather than the bottom electrode. The previous analysis can not explain the behavior of $G_P(V)$ in the whole bias voltage range well. Furthermore, when the bias voltage varies from 0 mV to V_c [from illustration B to illustration A in Fig. 1(c)], only the channel of majority spins opens and thus $G_P(V)$ should increase a little according to the density of state (DOS) of CFAS [15,16]. Nevertheless, $G_P(V)$ actually decreases slowly with bias voltage from 0 mV to V_c, as Fig. 1(b) shows.

In order to solve these problems, here we suggest another phenomenological explanation as follows. In the case that bottom electrode has half-metallic band structure and its spin polarization (P_1) is much larger than that of top electrode (P_2), the parallel configuration [illustration C in Fig. 1(c)] could be considered as a combination state of a large parallel configuration and a small antiparallel configuration [illustration D in Fig. 1(c)], since the states of s-like conduction electrons in bottom electrode and top electrode are not 100% parallel with each other. Note that a constant current was employed for every point on dI/dV-V curves and the sequentially changed constant current was kept with the same step for the whole measurement. Suppose electrons are tunneling from bottom to top, with increasing current, more and more electrons with majority spins are blocked at the interface due to the existence of the small antiparallel configuration, causing a larger and larger additional potential between the bottom electrode and top electrode until $V = V_c$. When $G_P(V)$ was plotted as a function of bias voltage, the additional potential was represented as the declining of $G_P(V)$ from 0 mV to V_c.

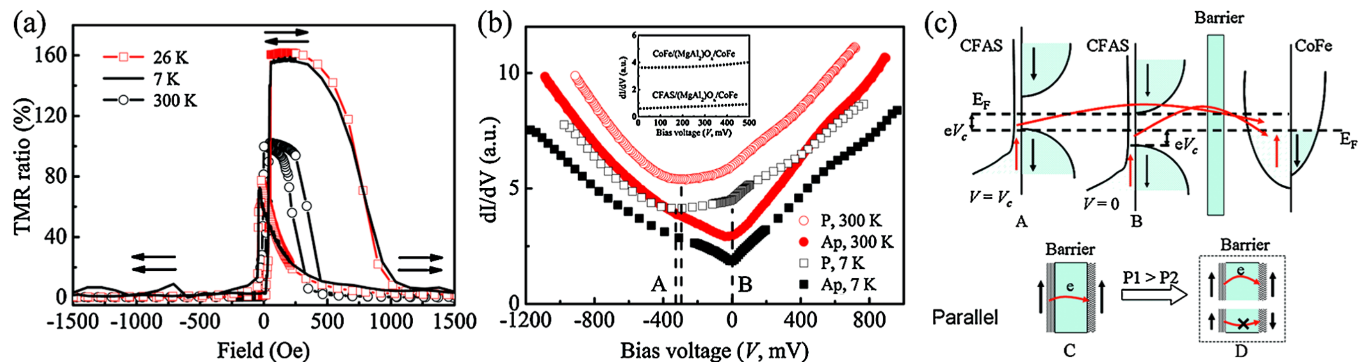

FIG. 1 (color online). (a) Magnetoresistance curves of CFAS/$(MgAl_2)O_x$/CoFe MTJs at 7, 26, and 300 K. (b) Dependence of differential conductance on bias voltage (dI/dV-V) of CFAS/$(MgAl_2)O_x$/CoFe MTJs for parallel and antiparallel configurations at 7 and 300 K. Dashed lines A are corresponding to the critical bias voltages (V_c), at which dI/dV curves show the minimum values for parallel configuration at 7 and 300 K; Dashed line B points to the bias voltage of 0 mV. The dependences of differential conductance of CFAS/$(MgAl_2)O_x$/CoFe MTJs and CoFe/$(MgAl_2)O_x$/CoFe MTJs for parallel configuration at 300 K on bias voltage (from 0 to 500 mV) are shown in the inset. (c) Schematic diagram of tunneling process of CFAS/$(MgAl_2)O_x$/CoFe MTJs at a finite bias voltage for parallel configurations.

Oppositely, the blocking effect disappears when electrons are tunneling from top to bottom because blocked electrons with minority spins could change spin states to majority spins more easily through spin flip in low P electrode. Accordingly, this explanation of the behavior of $G_P(V)$ in negative bias voltage range also points out a large gap between the Fermi level and the top of valence band of CFAS.

To reveal the band structure of CFAS more clearly, spin wave excitation model was adopted in this study. The original definition of spin polarization is: $P_0 = (D_M - D_m)/(D_M + D_m)$, where D_M and D_m stand for the DOS at the Fermi level for the majority and minority spins, respectively. In a half-metal, if the Fermi level position is very close to the edge of the valence band or the conduction band, a phenomenon called ''positive feedback'' may occur under the influence of thermal activity, leading to a collapse of the half-metallic property [6]. For simplicity, we describe P_0 as a temperature-related $P_0(T)$ with an integral of DOS from $E_F - k_BT$ to $E_F + k_BT$. According to this description, a material with a narrow band gap or a narrow energy separation between the Fermi level and the conduction or valence band edge smaller than the thermal activation energy k_BT is not a half-metal at temperature T. Finally, the decaying of P_{eff} could be written as $P_{\text{eff}} = P_0(T)(1 - \alpha T^{3/2})$, where the decay factor α is a material-dependent constant and may be affected by the circumstance of interface.

In general, the fitting of TMR ratio should use a modified Julliere's model which includes the contribution from the spin-independent conductance (G_{SI}) of MTJs [4]. However, we found that G_{SI} was negligibly small because of a crystallized barrier in our study. Cross-sectional high resolution transmission electron microscope (HRTEM) images of CFAS/$(MgAl_2)O_x$/CoFe multilayers are shown in Fig. 2(a). $(MgAl_2)O_x$ barrier clearly shows the crystalline feature, unlike the amorphous structure report by Sakuraba *et al.* [18] using a similar (Mg/Al)-O barrier. The nanobeam diffraction pattern shown in Fig. 2(b) clearly indicates that the bottom CFAS is $B2$ ordered, and that from the $(MgAl_2)O_x$ barrier [Fig. 2(c)] is consistent with spinel $MgAl_2O_4$ although it does not exclude the possibility of γ-Al_2O_3. The high-angle annular dark field (HAADF) image in Fig. 2(d) shows uniform thickness of each layer with dark contrast from the oxide barrier. The energy filter elemental maps for Al and Co [Figs. 2(e) and 2(f)] show that Al is uniformly distributed within the barrier layer sandwiched with CFAS and CoFe, suggesting intermixing of Mg and Al during the oxidation process of the barrier, which retarded the formation of separate MgO and Al_2O_3 layers. The crystallized $(MgAl_2)O_x$ brought an ideal barrier for spin-dependent tunneling ($G_{\text{SI}} = 0$) and a low RA of $1.7 \times 10^4\ \Omega\ \mu\text{m}^2$ for CFAS/$(MgAl_2)O_x$/CoFe magnetic tunneling junctions. Although the barrier with crystalline structure is formed, we do not believe that coherent tunneling occurs in our junctions because of the following reasons. First, the maximum TMR ratio of the MTJs with inserted Mg layer is the same as that of the MJTs fabricated under identical conditions except for a barrier without inserted Mg layer (amorphous AlO_x barrier) in Ref. [11]. Second, the behavior of $G_P(V)$ in our junction is quite different from that of MTJs with the contribution of coherent tunneling [20], while it is greatly in accord with the character of half-metal with large band gap.

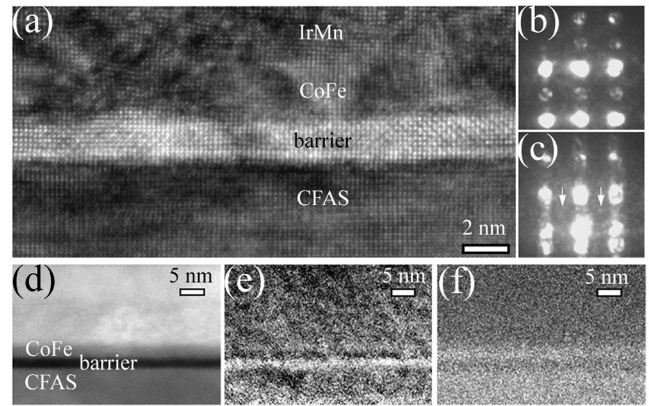

FIG. 2. (a) High resolution TEM image of an epitaxial $(MgAl_2)O_x$ barrier on $B2$-CFAS. $(MgAl_2)O_x$[100] axis is parallel with CFAS[110] axis in horizontal direction because of the small lattice mismatch between them. Both [001] axes of CFAS and $(MgAl_2)O_x$ are along the vertical direction. (b) Diffraction pattern taken in CFAS. (c) Diffraction pattern taken in barrier, {022} planes of spinel structure are indicated by arrows. (d) HAADF-STEM image. (e) EELS map of Al. (f) EELS map of Co. Mg map is absent because of the undistinguishing Mg region in the image.

Attributing to Fermi level tuning, $P_0(T)$ of CFAS should be a constant from 0 K to room temperature in our junctions. This inference is confirmed by the perfect agreement between experimental data and the fitting curve of temperature dependence of TMR ratio for CFAS/$(MgAl_2)O_x$/CoFe MTJs, as shown in Fig. 3(a). A CoFe/$(MgAl_2)O_x$/CoFe MTJs is employed to acquire $P_0(T)$ of CoFe pinned layer. The good fitting result for CoFe/$(MgAl_2)O_x$/CoFe MTJs is also plotted in Fig. 3(a). The fittings give values of $P_0(T)$ for CoFe and CFAS in MTJs at 300 K being 0.493 and 0.91, respectively. Compared with the poor performance of Co_2FeAl and Co_2FeSi, the high $P_0(T)$ of CFAS at room temperature clearly substantiates the success of Fermi level tuning in CFAS.

On the other hand, the values of α for CoFe (3 nm) film with exchange bias and CFAS (30 nm) film obtained from the magnetization versus temperature curves, such as the inset shown in Fig. 3(a), are only 3.5×10^{-6} and 4.3×10^{-6}, respectively, while those for CoFe and CFAS obtained by TMR effect are 2×10^{-5} and 3.2×10^{-5}, respectively. Such high values of α obtained by TMR effect are because TMR effect relies heavily on the magnetic properties of the upmost monolayer of electrodes at the

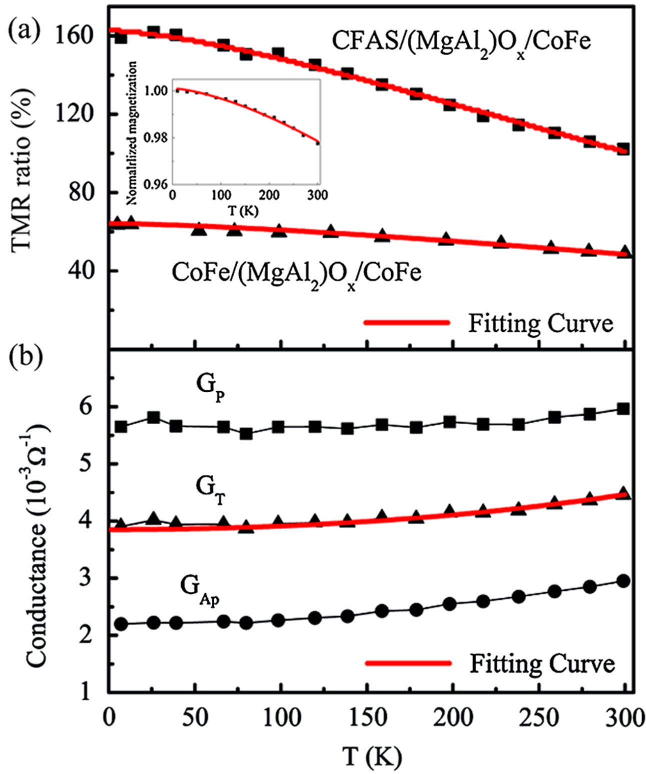

FIG. 3 (color online). (a) Temperature dependence of TMR ratio for CFAS/$(MgAl_2)O_x$/CoFe MTJs and CoFe/$(MgAl_2)O_x$/CoFe MTJs and the fitting curves by Bloch $T^{3/2}$ law. The inset shows the dependence of normalized magnetization on temperature from 10 to 300 K for CFAS (30 nm) single layer and the fitting curve by Bloch $T^{3/2}$ law. (b) Temperature dependence of G_P, G_{Ap} and G_T for CFAS/$(MgAl_2)O_x$/CoFe MTJs and the fitting curve of G_T, where G_P and G_{Ap} are the conductance of MTJs for parallel and antiparallel configurations, respectively; G_T is the prefactor for direct spin-dependent elastic tunneling.

interface [4], where the magnetization usually decays very fast [21]. Additionally, the large values of α than those reported elsewhere are also due to that other researchers neglected the temperature dependence of G_T, which is the prefactor for direct spin-dependent elastic tunneling with a function of $G_T = (G_P + G_{Ap})/2$ in the case that $G_{SI} = 0$, where G_P and G_{Ap} are the conductance of magnetic tunneling junctions for parallel and antiparallel configurations, respectively. The unreasonable assumption of G_T will bring a reduced α and a weaker temperature dependence of spin polarization. Figure 3(b) shows the temperature dependence of G_P, G_{Ap}, G_T for CFAS/$(MgAl_2)O_x$/CoFe MTJs, and the fitting curve of G_T using the formula (2) given in Ref. [4]. The fitting yields the barrier height $\phi = 0.82$ eV with an effective thickness of $(MgAl_2)O_x$ barrier being $t_{eff} = 20$ Å, while $\phi = 0.34$ eV with $t_{eff} = 13$ Å. To sum up, our work strongly suggests that α is as important as $P_0(T)$ to realize higher P_{eff}.

In conclusion, Fermi level tuning has been successfully demonstrated in CFAS. We believe that Fermi level tuning would be one of the essential techniques to achieve the materials with higher spin polarization for the spintronic device in future.

R. Shan would like to thank Dr. J. Qin of the School of Materials Science and Engineering at Shanghai University for her helpful discussions and advice. This work was partly supported by the NEDO, CREST, and JST-DFG project.

[1] R. A. deGroot, F. M. Mueller, P. G. van Engen, and K. H. J. Buschow, Phys. Rev. Lett. **50**, 2024 (1983).
[2] D. Mauri, D. Scholl, H. C. Siegmann, and E. Kay, Phys. Rev. Lett. **61**, 758 (1988).
[3] A. H. MacDonald, T. Jungwirth, and M. Kasner, Phys. Rev. Lett. **81**, 705 (1998).
[4] C. H. Shang, J. Nowak, R. Jansen, and J. S. Moodera, Phys. Rev. B **58**, R2917 (1998).
[5] C. Hordequin, D. Ristoiu, L. Ranno, and J. Pierre, Eur. Phys. J. B **16**, 287 (2000).
[6] J. J. Attema, G. A. deWijs, and R. A. deGroot, J. Phys. Condens. Matter **19**, 315212 (2007).
[7] Y. Sakuraba *et al.*, Appl. Phys. Lett. **88**, 192508 (2006).
[8] K. Inomata *et al.*, J. Phys. D **39**, 816 (2006).
[9] K. Inomata, S. Okamura, R. Goto, and N. Tezuka, Jpn. J. Appl. Phys. **42**, L419 (2003).
[10] T. Block *et al.*, J. Solid State Chem. **176**, 646 (2003).
[11] N. Tezuka *et al.*, Appl. Phys. Lett. **89**, 112514 (2006).
[12] T. Ishikawa *et al.*, Appl. Phys. Lett. **89**, 192503 (2006); N. Tezuka *et al.*, Appl. Phys. Lett. **89**, 252508 (2006).
[13] H. C. Kandpal, G. H. Fecher, and C. Felser, J. Phys. D **40**, 1507 (2007).
[14] N. Tezuka, N. Ikeda, S. Sugimoto, and K. Inomata, Jpn. J. Appl. Phys. **46**, L454 (2007).
[15] G. H. Fecher and C. Felser, J. Phys. D **40**, 1582 (2007).
[16] T. M. Nakatani *et al.*, J. Appl. Phys. **102**, 033916 (2007).
[17] Y. Sakuraba *et al.*, Appl. Phys. Lett. **89**, 052508 (2006).
[18] Y. Sakuraba *et al.*, J. Magn. Soc. Jpn. **31**, 338 (2007).
[19] M. Julliere, Phys. Lett. A **54**, 225 (1975).
[20] S. Tsunegi *et al.*, Appl. Phys. Lett. **93**, 112506 (2008).
[21] W. H. Wang *et al.*, Phys. Rev. B **71**, 144416 (2005).